A smart monitoring approach based on decentralized digital twins

Kosmas Dragos and Kay Smarsly

Institute of Digital and Autonomous Construction, Hamburg University of Technology, Blohmstraße 15, 21079 Hamburg, Germany
kosmas.dragos@tuhh.de

Abstract

The abundance of data, collected by sensors installed in civil engineering structures, has been fostering smart monitoring approaches that leverage digital twins, i.e. virtual representations that "live" and "evolve" in tandem with the physical structures. Conventional digital twins usually reside in centralized servers, which also serve as data collection hubs of sensor networks, installed in the structures. Therefore, the centralized servers facilitate the data exchange between the structures and the respective digital twins, essentially constituting the "single source of truth" regarding the structural condition. However, centralized digital twin (DT) approaches are inherently vulnerable to malfunctions of the server or data loss in wireless smart monitoring systems, which may end up being a "single point of failure". This paper aims to circumvent this problem by decentralizing digital twins into the microcontrollers of smart wireless sensor nodes. In particular, building on previous studies that utilize the embedded processing capabilities of smart wireless sensor nodes, a decentralized DT approach is proposed, in which the DT is segmented into partial digital twins that are embedded in the microcontrollers of the sensor nodes. By defining interfaces for data exchange, the wireless sensor nodes use the partial digital twins to collaboratively analyze the structural condition. The proposed approach is validated through experiments using a laboratory test structure, in which the decentralized DT is represented by a finite element model. The results of the tests demonstrate the capability of the decentralized DT approach to evolve with the physical structure, thus serving as an attractive solution for modern smart monitoring systems.

Keywords: Digital twins, smart monitoring, wireless sensor nodes, embedded computing, finite element modeling.

1 Introduction

Digitalization represents a growing trend in modern societies, with computer systems being employed in the majority of day-to-day activities [1]. In this direction, structural maintenance activities have been experiencing a transition from traditional manually executed inspections and tests to structural health monitoring (SHM), using sensor technologies for collecting digital structural response data and data analysis methods for extracting information on structural conditions [2, 3]. Furthermore, the technological advances in wireless communication have given rise to wireless SHM systems, exploiting the "cable-free" benefits of wireless sensor nodes [4], which, in turn, have fueled research in embedded-computing approaches, aiming to leverage the on-board processing capabilities of wireless sensor nodes for decentralizing and quasi-automating data analysis tasks [5, 6]. Embedded computing essentially grants wireless sensor nodes intelligence, thus converting wireless SHM systems into "smart monitoring" systems, capable of autonomously conducting SHM tasks.

Despite the momentum that SHM has gained in recent years, its methods largely remain of complementary fashion, primarily seeking to fill structural maintenance discontinuities, caused by intervals between successive on-site visual inspections and tests, and to provide the "reality" against which numerical models of structures are compared and updated [7]. Numerical models, e.g. finite element (FE) models, are particularly popular in SHM, owing to the intuitive way of mapping physical structures to FE meshes and to the easy integration of measurement locations into the meshes, which enables point-to-point comparisons between SHM data analysis outcomes and numerical simulation results. Even in smart monitoring systems, where embedded computing typically yields model-agnostic statistics or data-driven structural dynamic parameters, SHM outcomes are eventually compared with FE models for estimating the structural condition. Comparisons are usually accompanied by FE model updating, using optimization methods and artificial intelligence algorithms [8, 9], which provide information on the structural conditions and can be used for simulating future structural behaviors. Standard FE updating practice largely relies on fine-tuning global model parameters, e.g. material parameters, to minimize differences between simulation results and SHM data analysis outcomes, frequently represented by structural dynamic parameters, such as eigenfrequencies and mode shapes. To enhance FE model updating beyond global parameters, extending and fully integrating FE model updating into SHM strategies is necessary.

The concept of producing up-to-date FE models of structures using real-world structural response data from the structures is in line with the state-of-the-art paradigm of digital twinning, which has been increasingly employed in both industry and academia [10]. Digital twins constitute virtual representations of physical assets that "live" and "evolve" in tandem with the physical assets on the basis of continuous data exchange. In SHM, recent trends have been fostering approaches based on digital twins, in an attempt to make full use of structural response data collected by SHM systems [11]. In particular, digital twins are represented by FE models that are continuously updated, ideally in a near-real-time manner, which ensures the time-evolving attribute of the digital twins. Moreover, the tasks assigned to the digital twins may extend beyond FE model updating and encompass condition monitoring based on machine learning and big-data algorithms [12]. The end objective of a digital-twin-based approach in SHM is to provide a "single source of truth" for a structure being monitored, which can ultimately be used for estimating the remaining life of the structure.

Although research on digital twins for SHM is relatively new, a number of approaches have been proposed. Examples include the digital twin (DT) for bridge SHM, presented by Ye et al. [13], and the digital-twin-based representation of structural components over the service life, reported by Richstein et al. [14]. Dang et al. have introduced a machine-learning digital twinning approach for SHM, integrating cloud-based technologies [15]. In this direction, a DT for SHM combining machine learning and physics-based modeling has been introduced by Rito & Rochinha [16]. Furthermore, an example of transferring the DT concept to engineering practice is the "smartBRIDGE" project, implemented on Köhlbrand Bridge in Hamburg, Germany, in the framework of which the bridge is instrumented with a dense array of sensors and the digital twin has been developed to facilitate SHM and predictive maintenance [17]. An overview of DT applications in civil engineering, including SHM, has been provided by Bado et al. [18].

Despite the traction that digital twins have gained in SHM, the robustness of digital twins, particularly considering the aforementioned trend towards wireless SHM systems, remains an open challenge. The collection of structural response data in a centralized server runs the risk of converting the "*single source of truth*" to a "*single point of failure*" in the event of server malfunction or data loss, which is a frequent problem in wireless communication. To circumvent this challenge, this paper builds upon an alternative digital twinning concept, introduced in [19], by distributing the digital twins into the microprocessors of wireless sensor nodes. In particular, a smart monitoring approach is presented, in which digital twins are decentralized into wireless sensor nodes that are installed in the structure, as "partial digital twins", exploiting the embedded computing capabilities of the nodes. In other words, the digital twins being distributed become integral parts of the structure itself. The digital twins in this paper are realized as finite element models. First, a FE model of a structure being monitored is created and partitioned into partial FE models, each embedded in one wireless sensor node, following a concept originally introduced in [20]. The sensor nodes use the partial FE models and structural response data to collaboratively analyze the structural condition, with relatively minimal wireless communication. The proposed embedded DT approach is validated in laboratory experiments on a shear-frame structure, equipped with a wireless SHM system. The results showcase the capability of the embedded DT approach to detect and localize structural damage. In what follows, the methodology towards decentralizing digital twins is presented, followed by the implementation into a prototype SHM system. Next, the validation tests are presented, and the results are discussed. The paper ends with a summary and conclusions, followed by a brief outlook on potential follow-on research on this topic.

2 Decentralized digital twins for structural health monitoring

In the preliminary study presented in [19], digital twins have been realized as partial experimental mode shapes, extracted using data-driven modeling methods, which typically consist of vectors with low ranks equal to the number of measurement locations. As such, the digital twins are kept relatively "lightweight" and manageable for the limited computational resources of wireless sensor nodes. In this direction, the embedded digital twin approach, also attempts to keep the computational load low, by using reduced-order FE models for the decentralized digital twins. Therefore, this section, which presents the methodology of the embedded DT approach, first illuminates the method used for model order reduction (MOR), which is frequently employed in FE modeling to reduce the computational load, followed by the conversion of MOR results into instrumentation-compatible reduced-order models. Finally, the definition of decentralized digital twins from the instrumentation-compatible reduced-order models is described and the steps towards fulfilling SHM tasks using the decentralized digital twins are outlined.

2.1 Model order reduction

Following standard practice in structural engineering, MOR is applied as dynamic condensation via component mode synthesis (Craig-Bampton approach) [21]. Considering a finite element model of a civil engineering structure with N degrees of freedom subjected to vibration, the equation of motion is as follows:

$$\mathbf{M}^{N\times N}\ddot{\mathbf{x}}^{N\times 1}(t)+\mathbf{C}^{N\times N}\dot{\mathbf{x}}^{N\times 1}(t)+\mathbf{K}^{N\times N}\mathbf{x}^{N\times 1}(t)=\mathbf{p}^{N\times 1}(t), \tag{1}$$

where **M**, **C** and **K**, represent the mass, damping and stiffness matrix, respectively, and $\ddot{\mathbf{x}}$, $\dot{\mathbf{x}}$ and **x** denote the acceleration, velocity and displacement vectors, respectively, as functions of time t. On the right-hand side of Equation 1, **p** is the external force vector exerted on the structure. Dynamic condensation is applied by selecting a set of degrees of freedom to be kept ("retained" degrees of freedom – "b" set) and degrees of freedom to be condensed ("condensed" degrees of freedom – "a" set). For a civil engineering structure equipped with a wireless SHM system, it is reasonable to select the degrees of freedom being measured by the wireless sensor nodes as the b set. The matrices of Equation 1 are rearranged as follows (time notation is dropped for simplicity):

$$\left[\begin{array}{c|c}\mathbf{M}_{aa} & \mathbf{M}_{ab}\\ \hline \mathbf{M}_{ba} & \mathbf{M}_{bb}\end{array}\right]\left\{\begin{array}{c}\ddot{\mathbf{x}}_a\\ \hline \ddot{\mathbf{x}}_b\end{array}\right\}+\left[\begin{array}{c|c}\mathbf{C}_{aa} & \mathbf{C}_{ab}\\ \hline \mathbf{C}_{ba} & \mathbf{C}_{bb}\end{array}\right]\left\{\begin{array}{c}\dot{\mathbf{x}}_a\\ \hline \dot{\mathbf{x}}_b\end{array}\right\}+\left[\begin{array}{c|c}\mathbf{K}_{aa} & \mathbf{K}_{ab}\\ \hline \mathbf{K}_{ba} & \mathbf{K}_{bb}\end{array}\right]\left\{\begin{array}{c}\mathbf{x}_a\\ \hline \mathbf{x}_b\end{array}\right\}=\left\{\begin{array}{c}\mathbf{p}_a\\ \hline \mathbf{p}_b\end{array}\right\}. \tag{2}$$

The condensation of the a set consists in replacing submatrices $\mathbf{M}_{aa}$, $\mathbf{C}_{aa}$, $\mathbf{K}_{aa}$ with a set of generalized mass, damping and stiffness parameters obtained from the eigenvalue analysis of the submatrices with the degrees of freedom of the b set fixed (Craig-Bampton approach). Assuming that m eigenvalues are retained from the eigenvalue analysis of the submatrices (generally, $m << a$), the respective eigenvectors $\mathbf{\Phi}_{am}$ are combined with the static constraint modes $\mathbf{\Psi}_{ab} = (-\mathbf{K}_{aa})^{-1}\cdot\mathbf{K}_{ab}\cdot\mathbf{I}_{bb}$ into transformation matrix $\mathbf{\Psi}$:

$$\mathbf{\Psi}_b=\begin{bmatrix}\mathbf{\Phi}_{am} & \mathbf{\Psi}_{ab}\\ \mathbf{0}_{bm} & \mathbf{I}_{bb}\end{bmatrix}. \tag{3}$$

Finally, using the transformation matrix, the reduced-order model matrices $\tilde{\mathbf{K}}$, $\tilde{\mathbf{M}}$, consisting of b+m elements, are computed as $\tilde{\mathbf{K}} = \mathbf{\Psi}_b{}^T\mathbf{K}\mathbf{\Psi}_b$ and $\tilde{\mathbf{M}} = \mathbf{\Psi}_b{}^T\mathbf{M}\mathbf{\Psi}_b$.

2.2 Reduced-order models compatible with SHM instrumentations

The reduced matrices $\tilde{\mathbf{K}}$ and $\tilde{\mathbf{M}}$ have the following layout:

$$\tilde{\mathbf{K}}=\left[\begin{array}{c|c}\tilde{\mathbf{K}}_{bb} & \mathbf{0}_{bm}\\ \hline \mathbf{0}_{mb} & \mathbf{\Lambda}_{mm}\end{array}\right] \qquad \tilde{\mathbf{M}}=\left[\begin{array}{c|c}\tilde{\mathbf{M}}_{bb} & \tilde{\mathbf{M}}_{bm}\\ \hline \tilde{\mathbf{M}}_{mb} & \mathbf{I}_{mm}\end{array}\right], \qquad \mathbf{\Lambda}_{mm}=diag\left(\lambda_1,...,\lambda_m\right), \tag{4}$$

where $\lambda_r = \omega_r{}^2 = (2\pi f_r)^2$, for every $r = 1\ldots m$, are the eigenvalues computed from the eigenvalue analysis of the submatrices of the a set. With respect to damping, estimating the values of matrix **C** is a particularly challenging area of structural dynamics. Standard modeling and simulation practices suggest assuming **C** to be proportional to either matrix **M** or matrix **K** (or, in the general case, both **M** and **K**). In this study, **C** is assumed to be proportional only to the stiffness matrix **K**, resembling "structural damping"; extending the assumption to the reduced matrices, matrix $\tilde{\mathbf{C}}$ is computed according to the Rayleigh paradigm as $\tilde{\mathbf{C}} = \beta\tilde{\mathbf{K}}$, where $\beta = \xi_j/(\pi f_i)$ and ξ_j denotes the critical damping ratio of eigenmode j at frequency $f_j = \omega_j/2\pi$ of the reduced matrices. Using Equation 4, the resulting equation of motion for the reduced-order model is converted into:

$$\left[\begin{array}{c|c}\tilde{\mathbf{M}}_{bb} & \tilde{\mathbf{M}}_{bm}\\ \hline \tilde{\mathbf{M}}_{mb} & \mathbf{I}_{mm}\end{array}\right]\left\{\begin{array}{c}\ddot{\mathbf{x}}_b\\ \hline \ddot{\mathbf{q}}_m\end{array}\right\}+\beta\left[\begin{array}{c|c}\tilde{\mathbf{K}}_{bb} & \mathbf{0}_{bm}\\ \hline \mathbf{0}_{mb} & \mathbf{\Lambda}_{mm}\end{array}\right]\left\{\begin{array}{c}\dot{\mathbf{x}}_b\\ \hline \dot{\mathbf{q}}_m\end{array}\right\}+\left[\begin{array}{c|c}\tilde{\mathbf{K}}_{bb} & \mathbf{0}_{bm}\\ \hline \mathbf{0}_{mb} & \mathbf{\Lambda}_{mm}\end{array}\right]\left\{\begin{array}{c}\mathbf{x}_b\\ \hline \mathbf{q}_m\end{array}\right\}=\left\{\begin{array}{c}\mathbf{p}_b\\ \hline \mathbf{0}_m\end{array}\right\}, \tag{5}$$

where $\ddot{\mathbf{q}}$, $\dot{\mathbf{q}}$ and **q**, denote the acceleration, velocity and displacement vectors at the m generalized degrees of freedom. Equation 5 contains physical coordinates only of the b set, which, as mentioned previously, are the degrees of freedom measured by the wireless sensor nodes. Nevertheless, directly using Equation 5 is avoided in SHM systems, because (i) knowledge of displacement, velocity, and acceleration response data is required, which is usually unavailable, and (ii) the right-hand-side vector of forces is generally unknown. In most vibration-based SHM strategies, only acceleration

response data is measured, owing to the sensitivity of accelerations to high-frequency excitations [22]. It is therefore reasonable to express displacement and velocity response data with respect to acceleration response data; however, this expression is hardly possible in the time domain, because time integration of – generally – noisy acceleration response data would be required, which is frequently unstable [23]. Instead, for a time window of N_o measurements with time step Δt, Equation 5 is transformed into the frequency domain using the fast Fourier transform (FFT):

$$\mathcal{F}\left(\ddot{x}\right) = \ddot{X}\left(\omega_k\right) = \sum_{n=0}^{N_o-1} \ddot{x}_n \mathrm{e}^{-\mathrm{i}2\pi k\, n/N_o} \qquad k = \frac{\omega_k N_o \Delta t}{2\pi} \in \mathbb{Z}. \tag{6}$$

Applying Equation 6 for all acceleration response data of Equation 5, the frequency-domain representation of the equation of motion is obtained:

$$\left[\begin{array}{c|c} \tilde{\mathbf{M}}_{bb} & \tilde{\mathbf{M}}_{bm} \\ \hline \tilde{\mathbf{M}}_{mb} & \mathbf{I}_{mm} \end{array}\right] \left\{\begin{array}{c} \ddot{\mathbf{X}}_b\left(\omega\right) \\ \hline \ddot{\mathbf{Q}}_m\left(\omega\right) \end{array}\right\} + \beta \left[\begin{array}{c|c} \tilde{\mathbf{K}}_{bb} & \mathbf{0}_{bm} \\ \hline \mathbf{0}_{mb} & \mathbf{\Lambda}_{mm} \end{array}\right] \left\{\begin{array}{c} \dot{\mathbf{X}}_b\left(\omega\right) \\ \hline \dot{\mathbf{Q}}_m\left(\omega\right) \end{array}\right\} + \left[\begin{array}{c|c} \tilde{\mathbf{K}}_{bb} & \mathbf{0}_{bm} \\ \hline \mathbf{0}_{mb} & \mathbf{\Lambda}_{mm} \end{array}\right] \left\{\begin{array}{c} \mathbf{X}_b\left(\omega\right) \\ \hline \mathbf{Q}_m\left(\omega\right) \end{array}\right\} = \left\{\begin{array}{c} \mathbf{P}_b\left(\omega\right) \\ \hline \mathbf{0}_m \end{array}\right\}. \tag{7}$$

Furthermore, since the FFT produces summations of harmonic functions, the relationships between frequency-domain representations of displacement, velocity and acceleration response data are formulated as follows:

$$\dot{\mathbf{X}}\left(\omega\right) = \frac{\ddot{\mathbf{X}}\left(\omega\right)}{\omega i} + \varepsilon_1\left(\omega\right) \qquad\qquad \mathbf{X}\left(\omega\right) = -\frac{\ddot{\mathbf{X}}\left(\omega\right)}{\omega^2} + \varepsilon_2\left(\omega\right). \tag{8}$$

The error terms ε_1 and ε_2 are frequency-dependent and represent artifacts of the FFT, which is inherently approximative; for a precise artifact-free FFT, the exact values of the frequency content of the acceleration response data (e.g. the eigenmodes j) are required and must match the frequency "bins", represented by integer k in Equation 6, at which the FFT is computed. In practice, though, the frequency content is generally unknown ($k \neq j$).
With the help of Equation 8, the bottom part of Equation 7 yields:

$$\ddot{\mathbf{Q}}_m\left(\omega\right) = -\left(\mathbf{I}_{mm} + \frac{\beta}{\omega i}\mathbf{\Lambda}_{mm} - \frac{1}{\omega^2}\mathbf{\Lambda}_{mm}\right)^{-1} \tilde{\mathbf{M}}_{mb} \ddot{\mathbf{X}}_b\left(\omega\right). \tag{9}$$

Finally, using Equations 8 and 9, the upper part of Equation 7, containing only physical degrees of freedom of the b set, is obtained:

$$\begin{aligned} &\left[\left(\tilde{\mathbf{M}}_{bb} + \frac{\beta}{\omega i}\tilde{\mathbf{K}}_{bb} - \frac{1}{\omega^2}\tilde{\mathbf{K}}_{bb}\right) - \hat{\mathbf{M}}_{bb}\left(\omega\right)\right] \ddot{\mathbf{X}}_b\left(\omega\right) = \mathbf{h}_b\left(\omega\right) \\ &\hat{\mathbf{M}}_{bb}\left(\omega\right) = \tilde{\mathbf{M}}_{bm}\left(\mathbf{I}_{mm} + \frac{\beta}{\omega i}\mathbf{\Lambda}_{mm} - \frac{1}{\omega^2}\mathbf{\Lambda}_{mm}\right)^{-1} \tilde{\mathbf{M}}_{mb}. \end{aligned} \tag{10}$$

The vector $\mathbf{h}_b(\omega)$ is the frequency-dependent total error term, which contains the FFT-induced errors as well as the frequency-domain representations of the loads. The total error term is generally unknown and may affect the accuracy of Equation 10, similar to the limitation of the right-hand side of Equation 5, mentioned previously. In long-term SHM systems, the effect of the total error term may be compensated by modeling the error term using computational methods or machine learning algorithms. In any case, Equation 10 denotes an instrumentation-compatible reduced-order model, which is used for defining decentralized digital twins, as described in the next subsection.

2.3 Definition of decentralized digital twins

For defining the decentralized digital twins, the b set of degrees of freedom is partitioned into internal degrees of freedom u and interface degrees of freedom o. As such, Equation 10 is converted into:

$$\begin{bmatrix} \left(\begin{bmatrix}\tilde{\mathbf{M}}_{uu} & \tilde{\mathbf{M}}_{uo}\end{bmatrix}+\left(\frac{\beta}{\omega i}-\frac{1}{\omega^2}\right)\begin{bmatrix}\tilde{\mathbf{K}}_{uu} & \tilde{\mathbf{K}}_{uo}\end{bmatrix}-\begin{bmatrix}\hat{\mathbf{M}}_{uu}(\omega) & \hat{\mathbf{M}}_{uo}(\omega)\end{bmatrix}\right) \\ \left(\begin{bmatrix}\tilde{\mathbf{M}}_{ou} & \tilde{\mathbf{M}}_{oo}\end{bmatrix}+\left(\frac{\beta}{\omega i}-\frac{1}{\omega^2}\right)\begin{bmatrix}\tilde{\mathbf{K}}_{ou} & \tilde{\mathbf{K}}_{oo}\end{bmatrix}-\begin{bmatrix}\hat{\mathbf{M}}_{ou}(\omega) & \hat{\mathbf{M}}_{oo}(\omega)\end{bmatrix}\right) \end{bmatrix} \begin{bmatrix}\ddot{\mathbf{X}}_u(\omega) \\ \ddot{\mathbf{X}}_o(\omega)\end{bmatrix} = \begin{bmatrix}\mathbf{h}_u(\omega) \\ \mathbf{h}_o(\omega)\end{bmatrix}. \tag{11}$$

The degrees of freedom are partitioned following a "segmentation" logic, i.e. the reduced-order model is segmented into s "substructures" (partial models), each having internal degrees of freedom u_ν ($\nu = 1 \ldots s$) and being connected to other partial models via interface degrees of freedoms o. In the simplest case, the reduced-order model consists of two partial models each with one internal degree of freedom interconnected at interface degree of freedom $\bar{o}$. For partial model 1 with internal degree of freedom $w1$ ($u = [w1\ w2]$), the $w1$-th row of the upper part of Equation 11 is solved as:

$$\left(\begin{bmatrix}\tilde{\mathbf{m}}_{w1,u} & \tilde{m}_{w1,\bar{o}}\end{bmatrix}+\left(\frac{\beta}{\omega i}-\frac{1}{\omega^2}\right)\begin{bmatrix}\tilde{\mathbf{k}}_{w1,u} & \tilde{k}_{w1,\bar{o}}\end{bmatrix}-\begin{bmatrix}\hat{\mathbf{m}}_{w1,u}(\omega) & \hat{m}_{w1,\bar{o}}(\omega)\end{bmatrix}\right)\begin{bmatrix}\ddot{\mathbf{X}}_u(\omega) \\ \ddot{X}_{\bar{o}}(\omega)\end{bmatrix} = h_{w1}(\omega), \tag{12}$$

$$\ddot{X}_{\bar{o}}(\omega) = -\frac{\left[\tilde{\mathbf{m}}_{w1,u}+\left(\frac{\beta}{\omega i}-\frac{1}{\omega^2}\right)\tilde{\mathbf{k}}_{w1,u}-\hat{\mathbf{m}}_{w1,u}(\omega)\right]\ddot{\mathbf{X}}_u(\omega)-h_{w1}(\omega)}{\tilde{m}_{w1,\bar{o}}+\left(\frac{\beta}{\omega i}-\frac{1}{\omega^2}\right)\tilde{k}_{w1,\bar{o}}-\hat{m}_{w1,\bar{o}}(\omega)}. \tag{13}$$

In Equations 12 and 13, lower-case bold notations indicate one-dimensional vectors, and lower-case italics indicate matrix elements. From Equation 13, it follows that each row $w1$ of the equation of motion can be used for estimating the acceleration response data $\ddot{X}_{\bar{o}}$ at the interface degree of freedom $\bar{o}$. As a result, the row $w1$ is associated with partial model 1, which itself is defined as a decentralized DT. The estimates of $\ddot{X}_{\bar{o}}$ are used for decision making on the structural condition, as will be explained in the next subsection.

2.4 Structural condition assessment using decentralized digital twins

The assessment of structural condition using the decentralized digital twins essentially encompasses finding the reduced-order model that best fits the acceleration response data, recorded by the SHM system. As such, a family of reduced-order models is created by perturbing structural parameters $\boldsymbol{\theta}$ of the FE model, with each model resembling one prescribed structural damage scenario, and by applying Equations 1-13. Taking the two-partial-model example of Section 2.3, the $w1$-th rows of the family of reduced-order models are used to formulate a family of partial model 1 variants $\boldsymbol{\Theta}_{w1} = [\boldsymbol{\theta}_{w1,1}, \boldsymbol{\theta}_{w1,1}, \ldots, \boldsymbol{\theta}_{w1,L}]^T$ to be used by the respective decentralized DT. The variant that best fits the acceleration response data is found by comparing estimates $\ddot{X}_{\bar{o}}$ with actual structural response data $\ddot{Y}_{\bar{o}}$ at the interface degree of freedom, the comparison being formulated as an optimization problem using the following objective function:

$$\min_{\boldsymbol{\theta}_w} J = \sqrt{\frac{1}{\Omega}\sum_{\kappa=1}^{\Omega}\gamma\left|\ddot{X}_{\bar{o},\kappa}-\ddot{Y}_{\bar{o},\kappa}\right|^2}, \tag{14}$$

for a range of Ω angular frequencies. In Equation 14, γ is a weighting factor accounting for the contribution of the κ-th frequency to the structural response. A schematic description of the embedded DT approach is shown in Figure 1.

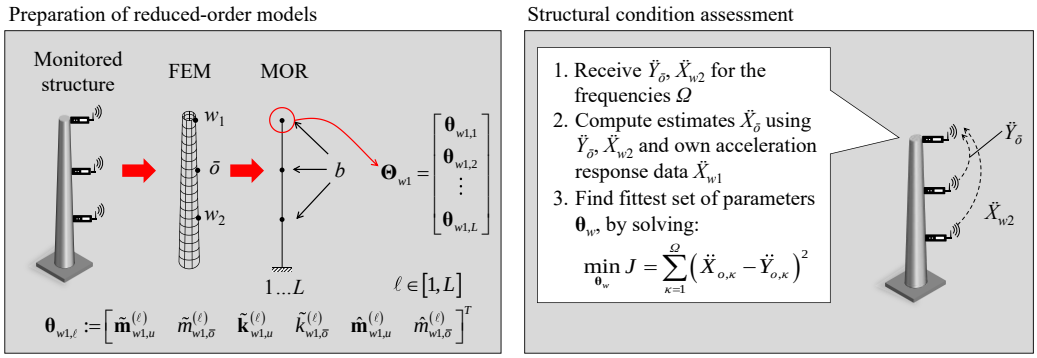

Fig. 1. Schematic overview of the embedded DT approach.

3 Implementation and validation

Implementation and validation tests are conducted as proof of concept for the embedded DT approach. Since the purpose of the tests is the proof of concept, the implementation, described first in this section, is kept at "prototyping" level and will be used as a basis for converting the embedded DT approach into a fully-fledged smart monitoring system in future research. The validation tests, showcasing the capability of the embedded DT approach in distinguishing between an "intact" structural condition and a "damaged" structural condition are presented thereafter.

3.1 Prototype implementation

The prototype implementation is illustrated in Figure 2. The first step entails preparing the family of reduced-order models. To this end, the structure being monitored is modeled using FE software that supports reduced-order modeling, and the family of reduced-order models is created by perturbing structural parameters for simulating structural damage scenarios. The typical outcome of MOR using FE software is a file containing the matrix elements $\boldsymbol{\theta}_{w1}$ (as shown in Figure 1); as a result, one file is created per structural damage scenario. Upon creating the files with the reduced-order model matrix elements, the files are read by software (to be embedded into the wireless sensor nodes) developed to implement Equations 13 and 14. Specifically, the software is written in Java programming language and consists of 5 main classes and 2 "helper" classes. The `FileReader` class reads files with matrix elements corresponding to the structural damage scenarios devised, and builds one `Scenario` object for each scenario. The `Scenario` class configures the matrix elements of $\tilde{\mathbf{K}}$ and $\tilde{\mathbf{M}}$, including both physical and generalized coordinates. The `Scenario` objects are stored into a "HashMap" in key-value format, allowing fast and easy retrieval of the objects. The `PartialModel` class applies Equation 13 for a given scenario to produce estimates $\ddot{X}_{\tilde{o}}$, using complex-valued frequency-domain representations of acceleration response data (necessary for applying Equation 13), received via the `DataTransceiver` class, e.g. data $\ddot{X}_{w2}$ in the two-partial-model example previously shown. Finally, the `Solver` class applies Equation 14 for each structural damage scenario, by accessing the respective `Scenario` object via its key in the HashMap and by creating a dedicated `PartialModel` object; the result of Equation 14 is the scenario (and the respective reduced-order model) that best fits the acceleration response data. The `Solver` class leverages the helper classes `FFT` and `Complex`, which are used for applying Equation 6 to acceleration response data recorded by the wireless sensor node and for performing complex-number operations, respectively.

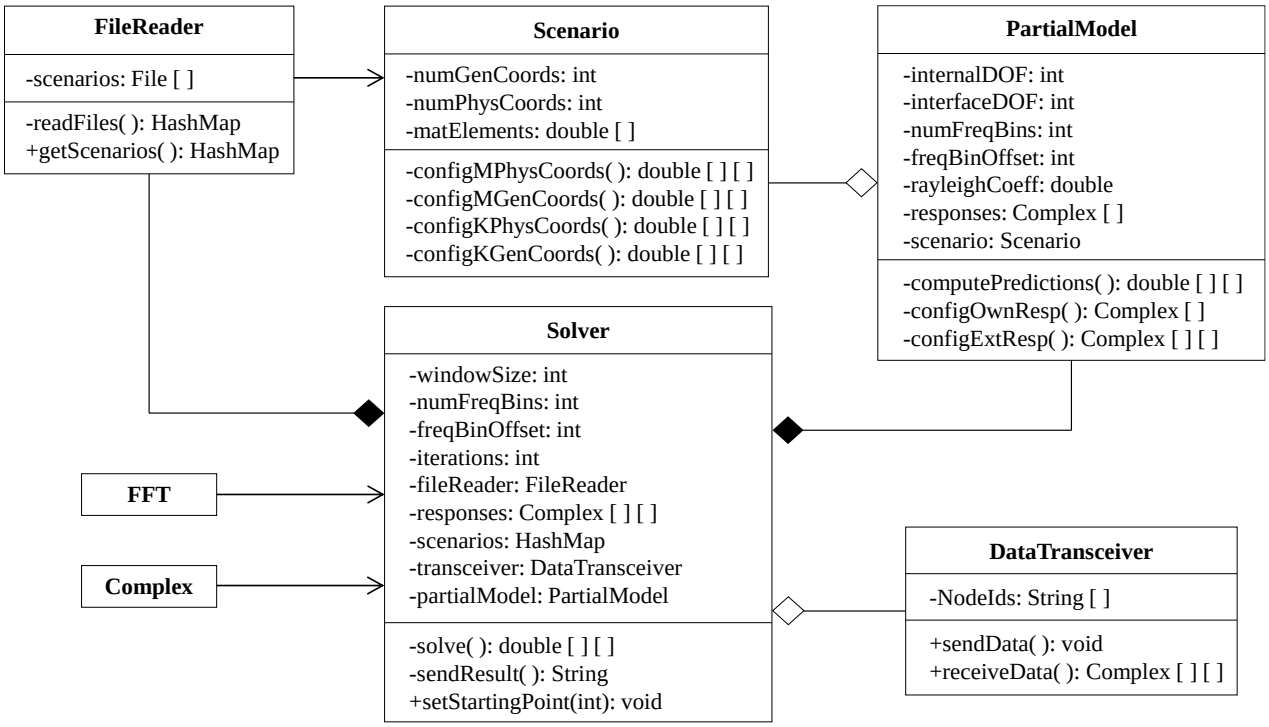

Fig. 2. Prototype software implementation of the embedded DT approach.

3.2 Laboratory validation tests

The laboratory tests, devised to showcase the capability of the embedded DT approach in detecting structural damage, are discussed in this subsection. First, the experimental setup is described, followed by the FE modeling conducted to create the digital twins. Finally, the tests are presented and the results are discussed.

Experimental setup. The laboratory validation tests are conducted on a down-scaled shear-frame structure, shown in Figure 3. The structure comprises 4 stories with slabs made of medium-density fiber that rest on 4 aluminum columns. The slabs are of dimensions 200×300×18 (mm) (width × length × thickness) and the columns are of rectangular cross sections with dimensions 20×1.7 (mm) (width × thickness). The vertical inter-story clearance is 245 mm. Slab-to-column connections are bolted with M4 bolts and considered partially fixed. The structure is fully fixed at its base on a 20-mm thick steel slab with dimensions 250×330 (mm) (width × length). The shear-frame structure is instrumented with 4 wireless sensor nodes of type Lord Microstrain G-Link-200 [24]. Each wireless sensor node is equipped with a triaxial micro-electro-mechanical-systems accelerometer, measuring accelerations at a configurable range up to ±8 g and at sampling frequencies up to 4,096 Hz. The accelerometers offer a 20-bit digital-output resolution and a noise floor of 25 μg/(Hz)$^{0.5}$. The wireless sensor nodes communicate with a base station of type Lord Microstrain WSDA-2000 ("data aggregator") over the license-free frequency of 2.405-2.48 GHz. Each wireless sensor node weighs 0.122 kg with the batteries on.

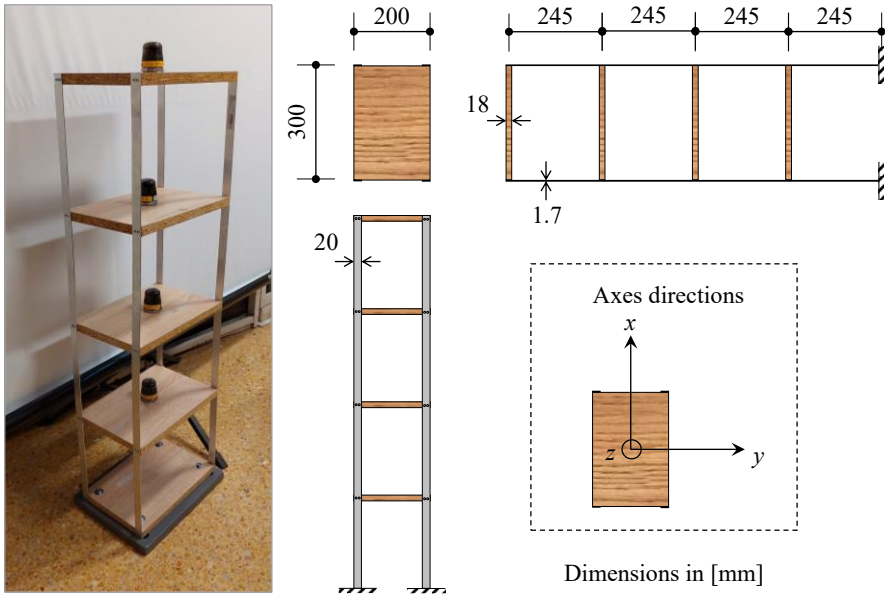

Fig. 3. Laboratory setup for the validation tests.

Finite element modeling and DT definition. The shear-frame structure is modeled using the finite element pre-processor software ANSA [25], as illustrated in Figure 4a. To avoid simplifications that would affect the accuracy of the decentralized digital twins, FE modeling is performed in an elaborate manner, using rectangular area elements both for the slabs and the columns. In particular, the middle surfaces of the slabs and columns are extracted and meshed. Slab-to-column bolted connections are modeled via beam elements of circular cross section, whose endpoints are attached to the columns and slabs via "rigid body elements" of type "RBE2". In each bolted connection, the RBE2 element implements a "master-slave" constraint between the beam-element endpoint (master) and the mesh grid points of the slab/column (slaves), thus ensuring fixity. As mentioned previously, bolted connections are considered partially fixed, because full fixity can hardly be – realistically – ensured. To account for the partial fixity, reduction factors for the "effective" diameter of the bolted connections are computed at each story, as part of model calibration against a set of preliminary acceleration response data. Upon calibrating the FE model, MOR is applied using the built-in "generate reduced representation" feature of the software. Specifically, special grid points ("loadcase points") that form the *b* set are defined at the center of each story, corresponding to degrees of freedom measured, which in these tests are only in the *x* direction; the rest of the grid points form the *a* set. Each reduced representation is created in the form of a "super-element", compatible with well-established FE practice [26], an example of which is shown in Figure 4b. Upon completing MOR, each super-element is illustrated by the loadcase points being retained, connected via blue straight lines that indicate the coupling between the degrees of freedom of the loadcase points. The black square boxes represent

the supports of the shear-frame structure. It should be noted that, despite the similarity of the super-element to a "stick" model, the degrees of freedom of the loadcase points are fully coupled, i.e. submatrices $\tilde{\mathbf{K}}_{bb}$ and $\tilde{\mathbf{M}}_{bb}$ are fully populated with non-zero elements.

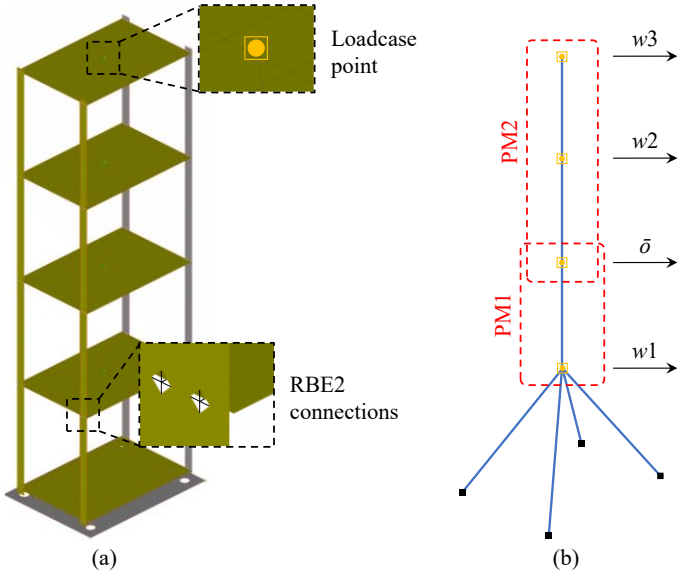

Fig. 4. (a) FE modeling of the shear-frame structure and (b) super-element created as reduced representation of the FE model.

One super-element is created for each structural damage scenario. A total of 5 super-elements are created, 4 of which represent structural damage scenarios, realized as loss of one slab-to-column connection per story, and 1 represents the intact shear-frame structure. The reasoning behind selecting only one slab-to-column connection per story for the damage scenarios is that the loss of any slab-to-column connection within the same story is expected to have identical impact on the reduced-order model, due to the double in-plane symmetry of the structure. For each super-element, the number of eigenvalues is set equal to $m = 16$, which is adequate for capturing the structural dynamics of the a set. The reduced representations are saved in "precompiled header" files (.pch), which are read by the embedded software. As can be seen from Figure 4b, two partial FE models are defined upon creating each super-element: PM1 with internal degree of freedom $w1$, and PM2 with internal degrees of freedom $w2$ and $w3$. The two partial models are interfaced in the second story with degree of freedom $\bar{o}$. The PM1 is assigned the first row of the equation of motion, corresponding to $w1$, and the PM2 is assigned the fourth row, corresponding to $w3$. Both partial models are tasked to apply Equation 13.

Laboratory tests. Two laboratory tests are conducted, one corresponding to the intact shear-frame structure and one after effecting damage on one slab-to-column connection on the third story. The modeling of the total error term is neglected in the laboratory tests presented herein, because excitation conditions are similar in both tests, and the effect of the error term on Equation 13 is expected to be low. Both tests are conducted for a sampling period of 6 minutes (360 s), at a sampling frequency of 128 Hz, resulting in 46,080 measurements in each set of acceleration response data.

Upon completing the measurements, the software reads the .pch files with the reduced-order model elements and applies Equation 13 with the classes previously described. The Rayleigh coefficient is set to $6.713 \cdot 10^{-4}$ (kNm/s) based on the first eigenfrequency of the structure $f_1 \approx 2.37$ Hz and a damping ratio $\xi = 5‰$. To reduce the effects of noise, the estimates of acceleration response data $\ddot{X}_{\bar{o}}$ are computed via "windowing", i.e. each partial model uses the acceleration response data of the internal degrees of freedom in windows of 4,096 measurements with 50% overlap between successive windows, and the estimates are computed as the averages of all windows. The same windowing process is applied to compute the actual acceleration response data $\ddot{Y}_{\bar{o}}$; thereupon, Equation 14 is applied to retrieve the scenario with the minimum J value. The range of frequencies Ω is case-specifically selected for each validation test and for each partial model. More specifically, the frequencies with the highest contribution to the vibration are selected, such that the FFT amplitudes at the respective degrees of freedom exceed a predefined threshold. In this paper, the threshold for each set of acceleration response data is defined as $\delta = \mu_{\text{FFT}} + \sigma_{\text{FFT}}$, where μ_{FFT} is the average FFT amplitude and σ_{FFT} is the standard deviation. The weighting factor γ_κ for the κ-th frequency ($\kappa \in \Omega$) is set equal to $\gamma_\kappa = |\ddot{Y}_{\bar{o},\kappa}|/\max|\ddot{Y}_{\bar{o}}|$. Excitation consists of combinations of hammer testing (on different stories) and free vibration, inflicted by deflecting the top story of the shear-frame structure and letting the structure vibrate freely. The results are shown in Table 1.

Table 1. Results of the laboratory tests.

	Test 1		Test 2	
Scenario	PM1 (J)	PM2 (J)	PM1 (J)	PM2 (J)
Intact structure	22.54	8.27	14.49	11.72
Damage 1st story	156.66	120.37	37.13	4.31
Damage 2nd story	188.46	197.31	28.72	4.48
Damage 3rd story	203.75	482.44	10.92	2.56
Damage 4th story	303.26	343.21	13.37	2.79

From the results shown in Table 1, it is evident that both partial models are able to correctly identify the structural condition of the shear-frame structure. In the first test, the lowest values for J are computed for the "Intact structure" scenario, and the differences from the J values of the damage scenarios are considerable, thus enhancing the confidence in the structural condition identification. In the second test, the minimum values of J from both partial models are correctly computed for the damage scenario of the third story, albeit with smaller differences from other scenarios, which may be attributed to the effects of the total error term in Equation 13. Nevertheless, the results clearly indicate the occurrence and location of structural damage.

4 Summary and conclusions

In civil engineering, digital twins are virtual representations of physical structures that live and evolve in tandem with the physical structures. Updating of the virtual representations is usually conducted using structural response data collected by sensors in a centralized repository (server). However, the centralized collection of structural response data may jeopardize the robustness of the digital twins, in cases of server malfunction or data loss. This paper has presented an approach on decentralized digital twins, compatible with state-of-the-art wireless smart monitoring systems. The proposed embedded DT approach builds upon segmenting digital twins into partial digital twins, which are embedded into the microcontrollers of wireless sensor nodes. Following up on conventional digital-twinning practice in civil engineering, the digital twins presented herein have been realized as finite element models; by extension, the partial digital twins have been represented by partial (FE) models, each containing internal degrees of freedom and connected to neighboring partial models via interface degrees of freedom. The partial models have been created via model order reduction, which yields partial models computationally manageable for the wireless sensor nodes. The wireless sensor nodes use the partial models, structural response data locally collected and structural response data exchanged with wireless sensor nodes from neighboring partial models to collaboratively analyze the structural condition. For each wireless sensor node, the analysis entails retrieving the partial model variant that best fits the structural response data from a family of partial model variants, created by perturbing structural parameters to simulate damage scenarios. The best-fit partial model variant is selected by solving an optimization problem between estimates of structural response data at the interface degrees of freedom computed by the partial models and the actual structural response data at the interface degrees of freedom. The embedded DT approach has been validated in laboratory tests using a 4-story shear-frame structure equipped with a wireless SHM system. First, the shear-frame structure has been modeled using finite element software, and reduced-order models have been generated for five scenarios, one resembling the intact structure and four simulating damage in one slab-to-column connection per story. Two tests have been conducted, one with the intact shear-frame structure and one after inducing damage in one slab-to-column connection on the third story. In both tests, the embedded DT approach has retrieved the best-fit partial model variant that corresponds to the correct scenario, demonstrating the capability of the proposed approach in correctly identifying the structural condition. However, the optimum of the best-fit partial model variant for the second validation test has been retrieved with marginal differences from the other variants, thus indicating that further investigation on the effects of the errors infiltrating the computations is necessary, representing a potential future research direction. Furthermore, the performance of the embedded DT approach implemented in real-world smart monitoring systems may be assessed in future research.

Acknowledgments

The authors would like to express their sincere gratitude for the generous support received from the German Research Foundation (DFG) under grant SM 281/20-1. Any opinions, findings, conclusions, or recommendations expressed in this paper are those of the authors and do not necessarily reflect the views of the DFG.

References

1. Henriette, E., Feki, M., & Boughzala, I., 2015. The shape of digital transformation: A systematic literature review. In: Proceedings of the 9th Mediterranean Conference on Information Systems. Samos, Greece, June 15, 2015.
2. Farrar, C.R. & Worden, K., 2006. An introduction to structural health monitoring. Philosophical Transactions of the Royal Society A, 365(1851), pp. 303–315.
3. Law, K.H., Smarsly, K., & Wang, Y., 2014. Sensor data management technologies for infrastructure asset management. In: Wang, M.L., Lynch, J.P. & Sohn, H. (eds.). Sensor Technologies for Civil Infrastructures. Pp. 3-32. Sawston, UK: Woodhead Publishing, Ltd.
4. Lynch, J.P. & Loh, K., 2006. A summary review of wireless sensors and sensor networks for structural health monitoring. The Shock and Vibration Digest, 38(2), pp. 91–128.
5. Dragos, K. & Smarsly, K., 2015. A comparative review of wireless sensor nodes for structural health monitoring. In: Proceedings of the 7th International Conference on Structural Health Monitoring of Intelligent Infrastructure. Turin, Italy, July 01, 2015.
6. Smarsly, K., Law, K.H., & König, M., 2011. Autonomous structural condition monitoring based on dynamic code migration and cooperative information processing in wireless sensor networks. In: Proceedings of the 8th International Workshop on Structural Health Monitoring 2011. Stanford, CA, USA, September 13, 2011.
7. Hola, J. & Schabowicz, K., 2010. State-of-the-art non-destructive methods for diagnostic testing of building structures – anticipated development trends. Archives of Civil and Mechanical Engineering, 3(10), pp. 5–18.
8. Zárate, B. & Caicedo, J.M., 2008. Finite element model updating: Multiple alternatives. Engineering Structures, 30(2008), pp. 3724–3730.
9. Lee, J.J., Lee, J.W., Yi, J.H., Yun, C.B., & Jung, H.Y., 2005. Neural networks-based damage detection for bridges considering errors in baseline finite element models. Journal of Sound and Vibration, 280(2005), pp. 555–578.
10. Van Der Horn, E. & Mahadevan, S., 2021. Digital Twin: Generalization, characterization and implementation. Decision Support Systems, 145(221), 113524.
11. Wagg, D.J., Worden, K., Barthorpe, R.J., & Gardner, P., 2020. Digital twins: State-of-the-art and future directions for modeling and simulation in engineering dynamics applications. ASCE-ASME Journal of Risk and Uncertainty in Engineering Systems, 6(2020), 030901.
12. Worden, K., & Green, P.L., 2017. A machine learning approach to nonlinear modal analysis. Mechanical Systems and Signal Processing, 84(2017), pp. 34–53.
13. Ye, C., Butler, L., Calka, B., Iangurazov, M., Lu, Q., Gregory, A., Girolami, M., & Middleton, C., 2019. A digital twin of bridges for structural health monitoring. In: Proceedings of the 12th International Workshop on Structural Health Monitoring. Stanford, CA, USA, September 10, 2019.
14. Richstein, R., Schmid, S., & Schröder, K.-U., 2022. Using SHM for the representation of structural components over their service life within digital twins. In: Proceedings of the 2022 European Workshop on Structural Health Monitoring. Palermo, Italy, July 4, 2022.
15. Dang, H.V., Tatipamula, M., & Nguyen, H.X., 2022. Cloud-based digital twinning for structural health monitoring using deep learning. IEEE Transactions on Industrial Informatics, 18(6), pp. 3820–3830.
16. Ritto, T.G. & Rochinha, F.A., 2021. Digital twin, physics-based model, and machine learning applied to damage detection in structures. Mechanical Systems and Signal Processing, 155(2021), 107614.
17. Hamburg Port Authority (2022). smartBRIDGE Hamburg. Available at https://www.homeport.hamburg/portfolio/smartbridge, accessed December 06, 2023.
18. Bado, M.F., Tonelli, D., Poli, F., Zonta, D., & Casas, J.R., 2022. Digital twin for civil engineering systems: An exploratory review for distributed sensing updating. Sensors, 22(9), 3168.
19. Smarsly, K., Dragos, K., & Kölzer, T., 2022. Sensor-integrated digital twins for wireless structural health monitoring of civil infrastructure. Bautechnik, 99(6), pp. 471–476.
20. Dragos, K. & Smarsly, K., 2017. Decentralized infrastructure health monitoring using embedded computing in wireless sensor networks. In: Sextos, A. & Manolis, G. D. (eds.). Dynamic Response of Infrastructure to Environmentally Induced Loads. Pp. 183-201. Cham, Switzerland: Springer International Publishing AG.
21. Bathe, K.-J. & Dong, J., 2014. Component mode synthesis with subspace iterations for controlled accuracy of frequency and mode shape solutions. Computers and Structures, 139(2014), pp. 28–32.
22. Park, J.-W., Sim, S.-H., Jung, H.-J., & Spencer Jr., B.F., 2013. Development of a wireless displacement measurement system using acceleration responses. Sensors, 13(7), pp. 8377–8392.
23. Stiros, S.C., 2008. Errors in velocities and displacements deduced from accelerographs: An approach based on the theory of error propagation. Soil Dynamics and Earthquake Engineering, 28(2008), pp. 415–420.
24. Microstrain Sensing, 2020. Microstrain Sensing product datasheet: G-Link-200. Williston, VT, USA: Parker Hannifin Corp.
25. BETA Simulation Solutions, 2018. ANSA: The advanced CAE pre-processing software for complete model build-up, Version 21.0.0. Lucerne, Switzerland: BETA CAE Systems International AG.
26. Gockel, M.A., 1981. Handbook for Superelement Analysis: MSC/NASTRAN (Version 61). Newport Beach, CA, USA: McNeal-Schwendler Corp.